



PERGAMON

*Acta mater.* Vol. 47, No. 4, pp. 1241–1253, 1999  
© 1999 Acta Metallurgica Inc.  
Published by Elsevier Science Ltd. All rights reserved.  
Printed in Great Britain  
1359-6454/99 \$19.00 + 0.00

PII: S1359-6454(98)00428-5

## DEFORMATION-ASSISTED DECOMPOSITION OF UNSTABLE Fe<sub>50</sub>Cu<sub>50</sub> SOLID SOLUTION DURING LOW-ENERGY BALL MILLING

J. XU<sup>†</sup>, G. S. COLLINS<sup>‡</sup>, L. S. J. PENG<sup>‡</sup> and M. ATZMON<sup>†,‡</sup>

<sup>†</sup>Department of Nuclear Engineering and Radiological Sciences, The University of Michigan, Ann Arbor, MI 48109-2104, U.S.A., <sup>‡</sup>Department of Physics, Washington State University, Pullman, WA 99164-2814, U.S.A. and <sup>‡</sup>Department Materials Science and Engineering, The University of Michigan, Ann Arbor, MI 48109-2104, U.S.A.

(Received 23 June 1998; accepted 29 November 1998)

**Abstract**—An unstable, f.c.c. Fe<sub>50</sub>Cu<sub>50</sub> solid solution was prepared using high-energy ball milling of an elemental powder mixture. It was used as a parent alloy for isothermal annealing or low-energy ball milling (LEBM), both at 373–523 K. Alloy evolution was analyzed by X-ray diffraction, Mössbauer spectroscopy and differential scanning calorimetry. LEBM significantly enhanced the initial decomposition rate, but the decomposition process was complex and not monotonic. At and below 423 K, the initial decomposition was completely reversed at later times. The results are interpreted in terms of an effective-temperature model proposed by Martin for irradiated alloys. A dynamic phase diagram in the effective temperature is presented, and used to explain the presence of a two-phase region under all milling conditions. The non-monotonic behavior is suggested to be a result of coupling between phase evolution and mechanical properties, leading to a time dependence of the effective temperature. © 1999 Acta Metallurgica Inc. Published by Elsevier Science Ltd. All rights reserved.

### 1. INTRODUCTION

Over the last decade, phase transformations induced by ball milling of metal alloy powders, such as amorphization, disordering of intermetallic compounds and formation of supersaturated solid solutions, have been studied extensively (for an overview see Refs [1–5]). In the majority of these investigations, the formation of phases far from thermodynamic equilibrium was explained using equilibrium thermodynamics (e.g. Refs [6–10]). While such a simplification may be useful in limiting cases, a more complete understanding requires thorough consideration of the kinetic parameters that determine the degree of departure from equilibrium. One crucial aspect of the kinetics is the enhancement of atomic diffusion due to point-defect formation during deformation [11,12]. The analogue in irradiated materials, radiation-enhanced diffusion (RED) [13], has been studied extensively, but there are relatively few direct studies of deformation-enhanced diffusion [14–16]. A qualitative confirmation of diffusion enhancement by deformation is given by the fact that elemental mixtures are observed to homogenize during milling at room

temperature [17], when equilibrium diffusivities are exceedingly low.

A thermodynamic description of the competition between an amorphous and crystalline phase under ball milling was suggested by Ma and Atzmon [18] for Zr–Al alloys. They studied phase formation during high-energy ball milling in Al<sub>x</sub>Zr<sub>100-x</sub> for 0 < x < 30. Within experimental resolution, the steady state always corresponded to a single phase, either hexagonal solid solution or amorphous, depending on the composition. The free energy was a concave function of composition, i.e. the common-tangent rule was not satisfied. The authors pointed out that these observations were consistent with free-energy minimization, if two-phase coexistence was prohibited.

Recently, the behavior of ball-milled alloys has been studied as a function of temperature and milling intensity [19,20]. In Ref. [19], the coexistence of amorphous and crystalline Ni–Zr phases of the same composition was studied. Order–disorder transformations in FeAl were the subject of Ref. [20]. The analysis of experiments in Ref. [20] was based on a balance between two opposing driving forces: external forcing driving the alloy away from equilibrium and back-diffusion toward equilibrium. It has been observed that despite the different nature of the externally forced ballistic jumps, ion irradiation or mechanical shearing, the phases

<sup>†</sup>Permanent address: State Key Laboratory of RSA, Institute of Metal Research, Chinese Academy of Sciences, Shenyang 110015, China.

<sup>‡</sup>To whom all correspondence should be addressed.

obtained in immiscible alloy systems are nearly the same [21,22]. Bellon and Averback [23] have performed numerical simulations of mechanical alloying of two immiscible elements by shearing. One of their observations was that alloying takes place when the shearing rate is sufficiently rapid so that decomposition by diffusion is negligible. While their results are important to the understanding of mechanical alloying, they do not explain the coexistence of supersaturated phases observed in some alloy systems.

Enhanced solubilities observed in driven alloys can be understood in terms of an earlier model by Martin [24], originally proposed for irradiation. Under competition between externally driven mixing and thermal back-diffusion toward equilibrium, Martin showed that the configuration of a regular binary solution would be the same as that in thermal equilibrium at the temperature

$$T_{\text{eff}} = T(1 + \tilde{\mathcal{D}}_{\text{Bal}}/\tilde{D}) \quad (1)$$

where  $T_{\text{eff}}$  is the effective temperature,  $T$  the actual temperature,  $\tilde{\mathcal{D}}_{\text{Bal}}$ , the effective ballistic diffusion coefficient and  $\tilde{D} = c_A D_B^* + c_B D_A^*$ .  $c_X^*$  is the atomic fraction of species  $X$  (A or B), and  $D_X^*$  its tracer diffusion coefficient. Note that  $\tilde{D}$  is not the chemical interdiffusion coefficient, which is equal to  $\tilde{D}$  times the thermodynamic factor [25]. An important aspect of equation (1) is the fact that  $\tilde{D}$  is enhanced by supersaturation of point defects. Under deformation, the enhancement is due to nonequilibrium point defects produced by nonconservative dislocation motion [26, 27].

Martin defined an effective free energy for a regular solution, given by

$$\varphi(c) = \Delta H(c) + k_B T_{\text{eff}}(c \ln c + (1 - c) \ln(1 - c)) \quad (2)$$

where  $c$  is the mole fraction of the solute,  $\Delta H(c)$  the enthalpy of formation of the phase, and  $k_B$  Boltzmann's factor. He showed that the solubility limits in phases were given by the common-tangent rule, applied to  $\varphi(c)$ . At low temperatures,  $T_{\text{eff}}$  decreases dramatically with increasing  $T$ , leading to decreasing solubilities, in qualitative agreement with experiment. Similarly, the order parameter in order-disorder alloys increases with temperature at low temperatures. Atzmon and Ma [28] and Klassen *et al.* [29] have suggested that Martin's model, originally developed for irradiation, can be used as an approximation for ball-milled alloys. The heterogeneity of the deformation process is obviously not considered in the model, but variation of the effective temperature with composition can be incorporated. The observations of Ma and Atzmon [4] are consistent with the effective-temperature model in the limit  $\tilde{\mathcal{D}}_{\text{Bal}}/\tilde{D} \rightarrow \infty$ . In this limit, "ballistic" mixing takes place, but thermal diffusion is frozen, so the alloy is homogeneous.

The effective temperature is infinite, and the two-phase coexistence region vanishes.

In order to improve the understanding of nonequilibrium phase formation, it is important to explore the range between the single-phase limit investigated by Ma and Atzmon [18] on the one hand, and thermal equilibrium on the other. A systematic study of two-phase equilibria between terminal crystalline solid solutions under ball milling has not been reported to date, but would provide opportunities for experimental tests of existing theories. Attempts at such an investigation were made in the immiscible Ag-Cu system [29] but the experimental results suggest departures from effective internal equilibrium, as discussed later. In the present work, Fe-Cu was selected as a model alloy system to examine the transformation kinetics and steady state during ball milling.

Mechanical alloying in the immiscible Fe-Cu system, which exhibits a positive heat of mixing, has been widely investigated in the past few years [7, 10, 30–51]. X-ray diffraction and TEM studies indicate that mechanical alloying results in a significant extension of mutual solubility of Fe and Cu relative to the equilibrium values. A single-phase f.c.c. solid solution forms in  $\text{Fe}_c\text{Cu}_{1-c}$  for  $c < 0.6$ , while for  $c > 0.8$  only b.c.c. solid solution was obtained. For  $0.6 < c < 0.8$ , the two phases coexist [7, 30, 35]. Atomic-level mixing of Fe and Cu in the milled alloys was further confirmed by means of Mössbauer spectroscopy [33, 42, 50] and extended X-ray-absorption fine-structure (EXAFS) [37–40]. The crystallite size in the supersaturated solutions is generally below 20 nm. A number of authors have also studied thermal decomposition of unstable Cu-Fe solid solutions [33, 36, 41–43, 52]. Two aspects of the observed behavior are not predicted by the equilibrium phase diagram. In f.c.c.  $\text{Fe}_{50}\text{Cu}_{50}$ , a nearly pure f.c.c.-Fe phase has been observed to form prior to precipitation of b.c.c.-Fe. In b.c.c., Fe-rich solid solutions, segregation of Cu to the grain boundaries [50] was observed.

The variable which is expected to affect phase equilibria the most is the temperature. However, during commonly used high-energy ball milling, significant local heating of the powder can result [53, 54], so that the powder temperature is uncertain and fluctuates in time. Therefore, a low-energy ball mill was employed in the present study, for which the powder temperature can be controlled to a good accuracy [55]. Since mechanical alloying of immiscible, elemental, powders in a low-energy ball mill is a sluggish process, homogeneous  $\text{Fe}_{50}\text{Cu}_{50}$  alloys formed by high-energy milling were employed in the present study. These were used as parent alloys to be subsequently milled in a low-energy ball mill at elevated temperatures, corresponding to quenches in  $T_{\text{eff}}$ . Both the kinetics of decomposition and the nature of the steady state were investigated.

## 2. EXPERIMENTAL PROCEDURE

Commercial elemental Fe and Cu powders (99.9% purity) with a particle size of  $45\ \mu\text{m}$  ( $-325$  mesh) were used as starting materials. Solid solutions of f.c.c.  $\text{Fe}_{50}\text{Cu}_{50}$  (numbers represent atomic percent) were prepared by high-energy ball milling of an elemental powder mixture for 24 h in a SPEX 8000 shaker mill cooled by forced air flow. The powder blend was loaded together with stainless steel balls at a ball-to-powder weight ratio of about 4:1 in a stainless steel vial under an argon atmosphere. Typically, about 7 g of the alloyed powders were obtained for each run. The mechanically-alloyed  $\text{Fe}_{50}\text{Cu}_{50}$  powder was used as the parent alloy for subsequent low-energy ball milling (LEBM) at elevated temperature. Note that all LEBM runs discussed in this paper were performed with such alloy powders formed by high-energy ball milling.

LEBM was carried out in a vibrating frame grinder, Fritsch Pulverisette 0. 5 g of alloyed  $\text{Fe}_{50}\text{Cu}_{50}$  powder were loaded into a hardened steel vial with a hardened steel ball, 5 cm in diameter. The vial was sealed with a Viton or Teflon gasket, evacuated to below  $10^{-3}$  Torr using a sorption pump and back-filled with purified argon gas to a pressure above 150 kPa, maintained by a continuous contact with the argon supply during milling. The milling temperature was controlled by means of a resistive heater and ranged from 298 to 523 K. The temperature was measured and controlled using a thermocouple attached to the vial bottom and was kept within  $\pm 0.5$  K of the set value. It is important to note that the heating of the powder by ball impact is estimated to be less than 1 K [55], so that the powder temperature is known within  $\pm 1$  K. Unless noted otherwise, the amplitude of vial vibration was set to 1 mm. To prevent gaseous contamination, all milling runs were performed for the desired period without interruption. The incorporation of Fe due to abrasion of the milling tools, determined using energy-dispersive X-ray analysis in a scanning electron microscope, was lower than 3 at.% for all of the samples used in the present work. Gaseous impurity contents were determined by LECO analysis at Ames Laboratory. Oxygen and nitrogen concentrations in the milled powders were less than 0.8 and 0.3 wt%, respectively, for all milling times.

The structure of the milled powders was analyzed by X-ray diffraction (XRD) with a Rigaku D/max diffractometer using monochromated Cu-K $\alpha$  radiation produced by a rotating-anode source. Sample powders were mounted after mixing with a small amount of vacuum grease. Peak positions and full width at half maximum were determined after fitting Lorentzian functions to the diffraction peaks. The lattice parameters were calculated using Cohen's method [56] with the (111), (200), (220), (311) and (222) peaks for the f.c.c. phase and the

(110), (200) and (211) peaks for the b.c.c. phase. Instrumental broadening was determined using a polycrystalline Si standard and employed to correct the peak-width data. Thermal analysis was carried out in a differential scanning calorimeter (Perkin-Elmer DSC 7). The samples were sealed in Au pans and scanned at a heating rate of 20 K/min up to 973 K, under flowing purified argon. The baseline was obtained after each scan by performing a second scan under identical conditions without changing the sample configuration. The error in integrated enthalpy release was determined from the standard deviation of several measurements.

Hyperfine structure and phases in a few samples were investigated using Mössbauer spectroscopy and the  $^{57}\text{Fe}$  probe [57]. This spectroscopy can detect phases of nanometer-size crystallites containing Fe in amounts greater than about one percent of the Fe present. Spectra were measured at room temperature in transmission using an MS-1200 Ranger Scientific spectrometer with laser interferometer for absolute determination of scanning velocity. The source was 25 mCi of  $^{57}\text{Co}$  in Rh with an extrapolated linewidth of 0.21 mm/s. Absorbers consisted of 20 mg/cm $^2$  of the alloy powder. Measurements were made on the parent alloy immediately after high-energy ball milling, after milling at 423 K for 240 h, and after subsequent ageing for 4300 h at room temperature. Each phase present in a sample provides a distinctive signal characterized primarily by its centroid velocity (isomer shift) and, for magnetic phases, a hyperfine magnetic field. The hyperfine field at a probe nucleus is aligned either parallel or antiparallel to the local magnetization. For the  $^{57}\text{Fe}$  probe, the magnetic field results in a splitting of the signal into a six-line pattern, or sextet. For a random distribution of the directions of the local magnetization, line intensities are in proportion with 3:2:1:1:2:3. Spectra were fitted to superpositions of magnetically split sextets and paramagnetic singlet lines. As described later, the phases observed include paramagnetic f.c.c.-Fe, ferromagnetic f.c.c.-CuFe, and a small amount of wüstite attributed to oxide contamination. No b.c.c.-Fe was detected in any of the spectra within a precision of about 0.5% of the Fe present.

## 3. RESULTS

### 3.1. Formation of f.c.c. solid solution in Fe-Cu alloy

Solid solutions of f.c.c.  $\text{Fe}_{50}\text{Cu}_{50}$  were prepared by high-energy ball milling of elemental Fe and Cu powder mixtures. After 24 h of milling, the peaks of b.c.c.-Fe have completely disappeared and the XRD patterns contain only the peaks of an f.c.c. phase [Figs 1(a) and (b), 0 h]. The diffraction lines are broadened, and the lattice parameter of the f.c.c. phase is  $0.3640 \pm 0.0003$  nm. For comparison,

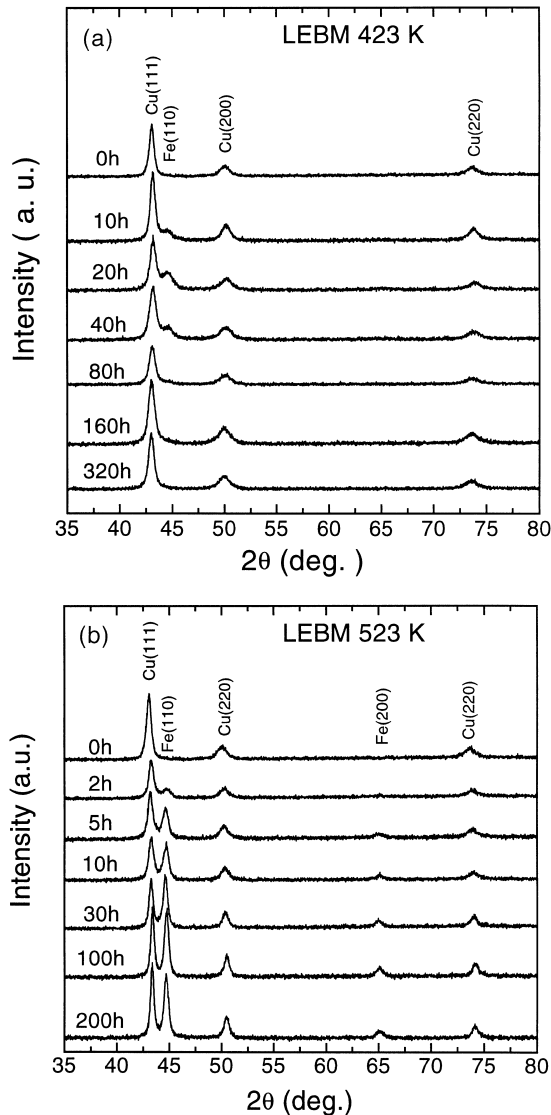


Fig. 1. X-ray diffraction patterns for parent alloy after different times of LEBM at: (a) 423 K; (b) 523 K.

the lattice parameter of the as-received pure Cu powder is 0.3615 nm, in agreement with the literature value [58]. Neglecting the contributions of strain and chemical heterogeneities to the (111) peak broadening, the Scherrer equation [59] yields a lower limit of 17 nm on the average grain size in the alloyed f.c.c. phase.

Milling may produce very small crystals of other phases in addition to the nanocrystalline grains of f.c.c.-CuFe. Since XRD is not sensitive to crystals smaller than several nm embedded in another [60], selected samples were examined by Mössbauer spectroscopy. Because the grains of the parent alloy were too thick to transmit the Mössbauer gamma rays, a sample was subjected to 10 h LEBM at room temperature. Based on extrapolation from other conditions, the short duration and low temperature are unlikely to have induced any signifi-

cant change in the phases. A Mössbauer spectrum of the parent alloy is shown in Fig. 2. The dominant feature in the figure is a broad distribution of hyperfine fields of the f.c.c.-CuFe phase. Empirically, the distribution was fitted well using two, broadened, component sextets. The hyperfine field at a particular probe nucleus depends on the moment of the probe atom as well as on the number of neighboring Fe atoms. The distribution is attributed to fluctuations in the moments and/or numbers of Fe neighbors. The bimodal character of the distribution could be caused either by a nonrandom distribution of Fe atoms in the alloy, by variations in the magnetic moments of Fe atoms depending on their local environments, or by composition fluctuations of the order of 1 at.%. It is not possible on the basis of the present experiments to distinguish between these causes. The spectrum was fitted with five components: (1) b.c.c.-Fe, with isomer shift, hyperfine field and linewidth fixed at values typical for the well-ordered bulk phase; (2) f.c.c.-Fe, using the isomer shift reported by Jiang *et al.* [32] and linewidth fixed to 0.25 mm/s; (3) and (4) the two components for the f.c.c.-CuFe phase; and (5) a paramagnetic phase whose fitted isomer shift is similar to that of the two lines of wüstite (FeO) and which is attributed to a small amount of oxidation. The characteristic isomer shifts and hyperfine fields of the phases and components are listed in Table 1. Fractions of the Fe content in the different phases are displayed in Table 1 for the parent alloy, as well as for two alloys milled 240 h at 423 K. Within experimental precision of about 0.3%, no b.c.c.-Fe was detected. For the parent alloy about 99% of the Fe is in the f.c.c.-CuFe phase. Good fits were only obtained by varying the ratio of intensity of the middle lines (lines 2 and 5) to the outer lines (lines 1 and 6) in the fits. Fitted line intensities were in proportion with 3:1.12:1:1:1.12:3. The reduced intensity of lines 2 and 5 arises from a net alignment of local magnetizations to the gamma-ray axis, that is, normal to the surface of the absorber. The cause of this alignment is unknown, but has similarly been observed

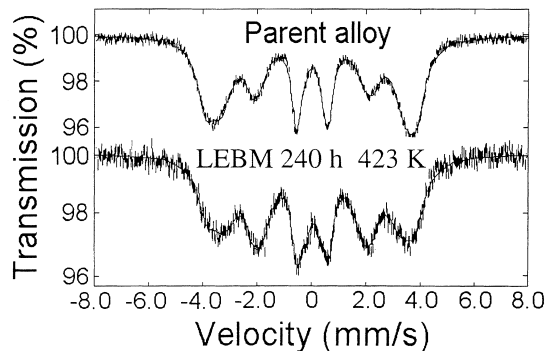


Fig. 2. Mössbauer spectrum for the parent alloy and sample milled 240 h at 423 K.

Table 1. Phases observed in Mössbauer spectra and percentages of Fe in three Fe<sub>50</sub>Cu<sub>50</sub> samples. Phases are characterized by their hyperfine field and isomer shift. Isomer shifts are with respect to b.c.c.-Fe at room temperature. Parameters fixed in the fits are in parentheses.

Phase	Hyperfine field (kOe)	Isomer shift (mm/s)	Parent alloy	Milled at 150°C, 240 h	Milled at 423 K, 240 h and aged at room temp. 4300 h
b.c.c.-Fe	(330)	(0.000)	-1.0(3)	-0.1(4)	-0.3(3)
f.c.c.-Fe	(0)	-0.11(2)	0.5(1)	2.1(3)	1.8(3)
f.c.c.-CuFe (I)	204(3)	+0.12(1)	64(5)	70(10)	73(8)
f.c.c.-CuFe (II)	238(2)	+0.09(1)	35(4)	24(7)	23(5)
wüstite	(0)	+0.30(3)	0.8(2)	4(1)	2(1)

in other as-prepared CuFe alloys [32, 61]. The spectrum of the parent alloy is quite similar to that observed by others after high-energy ball milling at room temperature (e.g. Ref. [32]) apart from the complete absence of b.c.c.-Fe and nearly complete absence of f.c.c.-Fe. It is possible, but not likely, that small amounts of b.c.c.-Fe and f.c.c.-Fe have been dissolved into the CuFe alloy by the 10 h LEBM at room temperature used to prepare the Mössbauer absorbers.

DSC analysis of the parent alloy shows a broad exothermic signal extending from 393 to 963 K, as seen in Fig. 3, where labeled according to the LEBM time of 0 h. Integration of the area under the DSC curve yields a total stored enthalpy of  $12.7 \pm 0.39$  kJ/mol. The lattice parameter and stored enthalpy we obtain are close to previously reported values [7, 10, 30, 32–37, 40, 42, 45], where small differences can be attributed to the different types of mills used. In summary, we conclude that the Fe<sub>50</sub>Cu<sub>50</sub> alloy produced by high-energy ball milling in this work is a f.c.c. solid solution.

### 3.2. Decomposition of FeCu solid solution during LEBM

The previously described Fe<sub>50</sub>Cu<sub>50</sub> parent alloy was used in all subsequent investigations. The XRD patterns for Fe<sub>50</sub>Cu<sub>50</sub> alloys after different LEBM times at 423 and 523 K are presented in Figs 1(a) and (b) as typical examples. The (110) peak of a b.c.c. phase appears after milling for 5 h at 423 K

and for 2 h at 523 K, and other reflections are visible at later times. In all cases, the lattice parameter of the b.c.c. phase is close to the literature value for pure b.c.c.-Fe. The lattice parameter of the f.c.c. alloy and the integrated Fe(110) to Cu(111) peak intensity ratio as a function of milling time, for temperatures ranging from 373 to 523 K, are shown in Figs 4 and 5, respectively. Variations due to texture are likely to be small because the mounting method is unlikely to lead to preferred orientation. It can be seen that at 523 K, the intensity ratio rapidly increases with milling time, then saturates after 30 h. Further milling does not cause a visible change. At the same time, the lattice parameter of the f.c.c. phase approaches a steady-state value after 100 h, which is close to the value for pure Cu, 0.3615 nm [58]. For samples milled at 423 K, the intensity ratio increases in the early stages and reaches a maximum at about 20 h, then drops and approaches zero after milling for 150 h. In the same samples, the lattice parameter decreases and reaches a minimum at about 20 h, subsequently increasing after about 80 h to a steady-state value equal to that for the parent alloy. A similar reversal is observed in all samples milled at  $373 \text{ K} \leq T \leq 473 \text{ K}$ , but the initial values of the lattice parameter and intensity ratio are recovered only for  $T \leq 423 \text{ K}$ . Note that the rate of initial evolution is similar for  $423 \text{ K} \leq T \leq 473 \text{ K}$ .

The evolution of the stored enthalpy during LEBM was monitored by DSC. Scans obtained after different LEBM times at 423 K are shown in

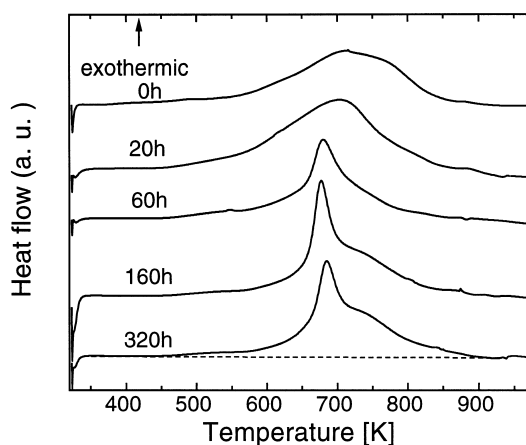


Fig. 3. DSC scans after different LEBM time at 423 K (heating rate 20 K/min).

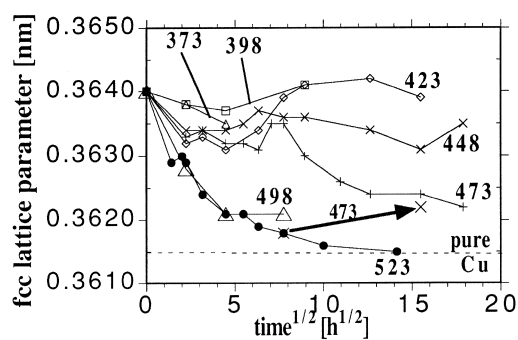


Fig. 4. Lattice parameters of the f.c.c. phase vs square root of LEBM time at different temperatures. The error is about  $\pm 0.0002$  nm. Milling temperatures in K are indicated, and arrow represents 523  $\rightarrow$  473 K milling sequence (see text).

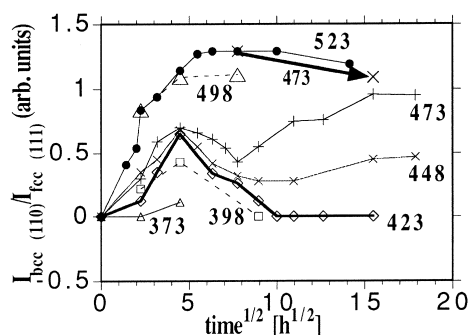


Fig. 5. Fe(110) to Cu(111) peak intensity ratio vs square root of LEBM time at different temperatures. The notation is the same as in Fig. 4.

Fig. 3 for a typical set of samples. Figure 6 shows the total stored enthalpy, obtained by integration of the DSC curves, at different temperatures as a function of LEBM time. For  $T \leq 473$  K, an initial decrease is subsequently reversed. For  $T \leq 423$  K, the initial value is essentially recovered at long times. In all cases, a steady-state value is approached for long times, the value of which decreases with increasing temperature. It is interesting to note that the exothermic DSC peaks for samples milled for long times at 423 K extend over a narrower temperature range than for the nominally identical parent alloy (see Fig. 3). Similarly narrow DSC peaks were observed for all samples subjected to LEBM at 473 K and below.

In order to confirm that the observed state after long milling time corresponds to a history-independent steady state, a temperature cycling experiment was conducted. An alloy milled for 60 h at 523 K was subsequently milled for 180 h at 473 K without being exposed to the atmosphere. The evolution during the second stage is indicated by arrows in Figs 4–6. It is apparent that the behavior is reversible and the steady state corresponding to 473 K is approximately obtained.

The full width at half maximum (FWHM) of the (111) Bragg peak of the f.c.c. phase is displayed as a function of time at different temperatures in Fig. 7. For  $T \leq 473$  K, an initial decrease from  $0.5^\circ$  to  $0.4^\circ$  is reversed after 5 h and a steady-state value of  $0.5^\circ$ – $0.6^\circ$  is reached at all temperatures. At 523 K, the FWHM remains unchanged for 10–20 h and then decreases to about  $0.35^\circ$ . The FWHM of the b.c.c. (110) peak of the precipitating phase shows little temporal change for  $448 \text{ K} \leq T \leq 523 \text{ K}$ , with values between  $1^\circ$  at the lowest and  $0.5^\circ$  at the highest temperature. For  $T \leq 423$  K, the FWHM increases to several degrees as the b.c.c. phase is dissolved.

†The spectral components of the CuFe phase in figs 2(a) and (c) of Ref. [32] are very similar to the spectra shown in our Fig. 2.

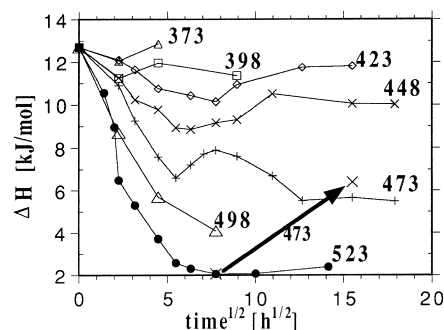


Fig. 6. Stored enthalpy vs square root of LEBM time at different temperatures. The error is 0.1–0.4 kJ/mol. The notation is the same as in Fig. 4.

Mössbauer measurements were performed after milling a sample of the parent alloy at 423 K for 240 h (see Table 1). Recall that for the parent alloy, no b.c.c.-Fe was detected to within a precision better than 0.5%. The amount of Fe in the f.c.c.-Fe phase increased slightly, from about 0.5 to 2%. Similarly, the amount of Fe in the wüstite-like oxide phase increased from about 1 to 3%. For the dominant f.c.c.-CuFe phase, there were two notable changes. First, the intensity of the lower field component (204 kOe) increased at the expense of the higher-field component (238 kOe). This is attributed to the removal of about 3.5% of Fe from the CuFe phase to form the f.c.c.-Fe and wüstite phases, and could be explained by any of the three possible causes of the bimodal distribution described earlier for the parent alloy. Second, the intensity ratios of the six lines of the sextet after LEBM fit very close to 3:2:1:1:2:3, indicating the elimination of significant magnetic texture observed in the parent alloy. Similar changes in magnetic texture have been observed in other studies after annealing CuFe samples near the 50:50 composition. In both the experiments of Jiang *et al.* on ball-milled FeCu† [32] and Sumiyama *et al.* on sputtered FeCu [61], significant texture with magnetization aligned normal to the plane of the sample surface was observed in the

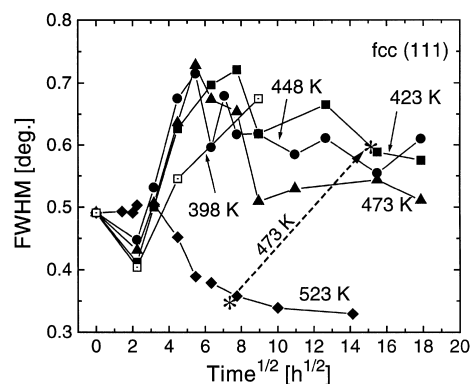


Fig. 7. FWHM of f.c.c. (111) peak vs square root of LEBM time at different temperatures. The notation is the same as in Fig. 4.

samples as prepared at or near room temperature. Annealing at 673 K led in both studies to elimination of the texture. Thus, although the origin of the magnetic texture and how it is removed are not understood in detail, LEBM at 423 K appears to lead to processes comparable to those observed after thermal annealing close to 673 K. Finally, note that subsequent ageing at room temperature for 4300 h produced no noticeable change in the Mössbauer spectrum (see Table 1).

From XRD and Mössbauer results, the behavior of the b.c.c.-Fe phase can be summarized as follows. It precipitates at all milling temperatures at similar rates. For  $T \leq 473$  K it is subsequently redissolved, and for  $T \leq 423$  K it disappears completely. After milling times ranging from 150 to 250 h, steady states are achieved.

Several milling runs were performed using a vibration amplitude of 1.5 mm at  $T = 398$  and 523 K. At 523 K, the observed evolution was similar to that at an amplitude of 1 mm. At 398 K, the degree of initial precipitation was significantly smaller, and it was reversed earlier, after 5–20 h.

### 3.3. Comparison with isothermal annealing

In order to evaluate the effect of milling on decomposition, isothermal anneals were conducted at 473 and 523 K for comparison with the milling experiments. At both temperatures, a b.c.c. phase is observed to form, and its diffracted intensity increases with time. Figures 8–10 show the integrated b.c.c. (110) to f.c.c. (111) Bragg peak intensity ratio, the lattice parameter of the f.c.c. phase, and the stored enthalpy, respectively, as a function of LEBM or annealing time at 473 and 523 K. In all cases, the precipitation of b.c.c.-Fe is accompanied by a decrease in the f.c.c. lattice parameter and in the stored enthalpy. At both temperatures, LEBM leads to a significantly higher

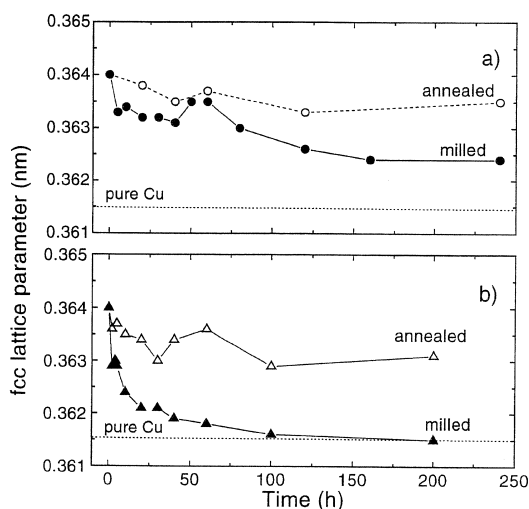


Fig. 8. Lattice parameters of f.c.c. phase vs time for LEBM or annealing at: (a) 473 K; (b) 523 K.

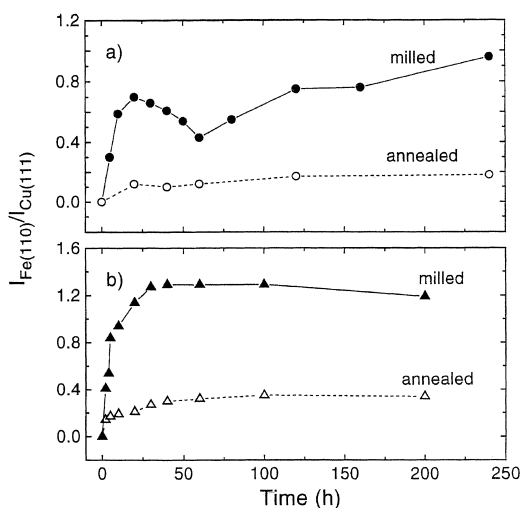


Fig. 9. Fe(110) to Cu(111) peak intensity ratio vs time for LEBM or annealing at: (a) 473 K; (b) 523 K.

decomposition rate. At 473 K, the time scale for reaching the equilibrium state of nearly pure terminal solutions by annealing appears to be orders of magnitude greater than the time scale of the experiment. Note that during annealing, the evolution of the lattice parameter is non-monotonic, but the b.c.c. (110) to f.c.c. (111) Bragg peak intensity ratio and the stored enthalpy are monotonic.

### 3.4. Effect of milling temperature on the steady-state

The steady-state values of the f.c.c. lattice parameter, Fe(110) to Cu(111) Bragg-peak intensity ratio and total stored enthalpy are shown in Figs 11(a)–(c), respectively, as a function of LEBM temperature. Data for short milling time are also plotted for comparison. With increasing milling temperature, the steady-state volume fraction of the

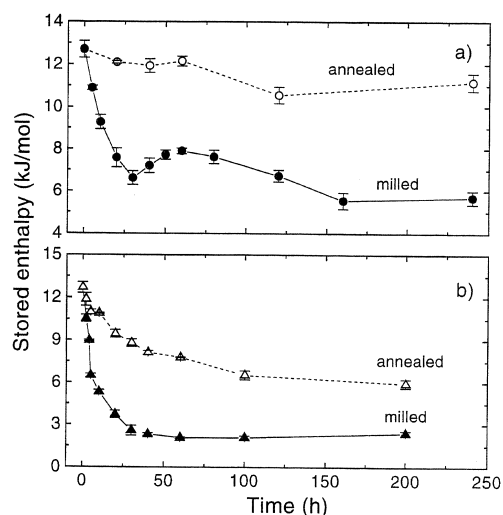


Fig. 10. Stored enthalpy for  $\text{Fe}_{50}\text{Cu}_{50}$  alloy vs time for LEBM or annealing at: (a) 473 K; (b) 523 K.

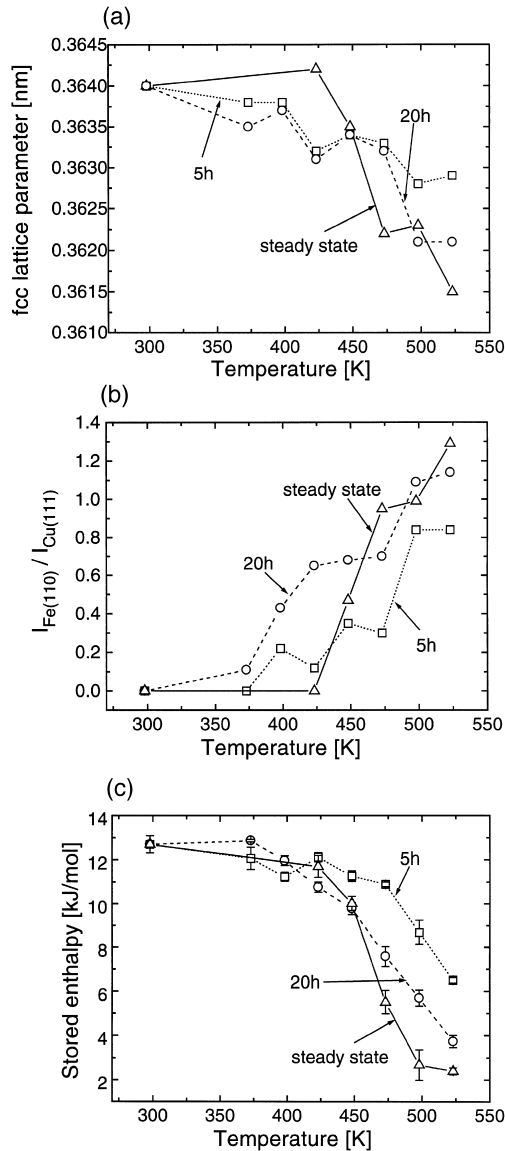


Fig. 11. (a) Lattice parameter of the f.c.c. phase vs milling temperature. (b) Fe(110) to Cu(111) peak intensity ratio vs milling temperature. (c) Stored enthalpy vs milling temperature after LBM for 5 h, 20 h and at steady state.

b.c.c. phase increases, and the stored enthalpy and lattice parameter of the f.c.c. phase decrease.

#### 4. DISCUSSION

In order to understand the effective thermodynamics corresponding to our experiments, a dynamic Cu–Fe phase diagram in  $T_{\text{eff}}$  (Fig. 12) has been calculated, using equation (2). The reader is reminded that  $T_{\text{eff}}$  decreases with increasing milling temperature. Note that this phase diagram depends on the milling conditions through  $T_{\text{eff}}$ . Values of  $\Delta H(c)$  for the f.c.c. and b.c.c. phases were determined from fits to the enthalpy data of Ma *et al.* [35]. For simplicity,  $T_{\text{eff}}$  was assumed to be independent of the

composition and crystal structure. Note that this assumption is not accurate for the present experiments, for which the steady-state solubility in the precipitating b.c.c. phase is significantly lower than that in the f.c.c. phase, in contrast to Fig. 12. It should be noted that  $T_{\text{eff}}$  for crystalline phases can often be significantly higher than their melting point, as implied by the observed high degree of supersaturation. The present LBM experiments at elevated temperatures correspond to quenches in  $T_{\text{eff}}$  from the f.c.c. single-phase region (e.g. at  $T_{\text{eff}}^1$ ) to lower values of  $T_{\text{eff}}$  (e.g.  $T_{\text{eff}}^2$ ) corresponding to the two-phase region, where precipitation of the b.c.c. phase is expected (see arrow in Fig. 12). Two important assumptions underlying the determination of the dynamic phase diagram are emphasized here: (1) The effective-temperature model applies to regular solutions or order–disorder alloys. It is not sufficiently sophisticated to determine the relative stabilities of b.c.c. and f.c.c. phases of the same composition. Since no f.c.c., Fe-rich, phase is observed at steady state, we assume that such a phase has a high effective free energy and can be ignored in the dynamic phase diagram. (2) Since an amorphous phase is not observed in this system,  $T_{\text{eff}}$  of a liquid/amorphous phase is assumed here to be sufficiently low so that its effective free energy is high and it does not compete with the crystalline phases. Therefore, the high- $T_{\text{eff}}$  behavior in Fig. 12 is never observed in equilibrium, where melting interferes with the solid phases.

Because the slopes of the enthalpy curves of the two phases at the point of intersection are different, a two-phase coexistence region is obtained for any value of  $T_{\text{eff}}$ , although its width decreases with increasing  $T_{\text{eff}}$ . To the authors' best knowledge, this dynamic phase diagram provides the first explanation of previous observations of a two-phase region in the Cu–Fe system for all milling conditions. Hong and Fultz [51] observed that, when using one value of milling intensity, the width of the two-phase coexistence region is reduced drastically from the equilibrium value, whereas an increase of the power input by a factor of 5.2 leads to a very small incremental change. In addition to

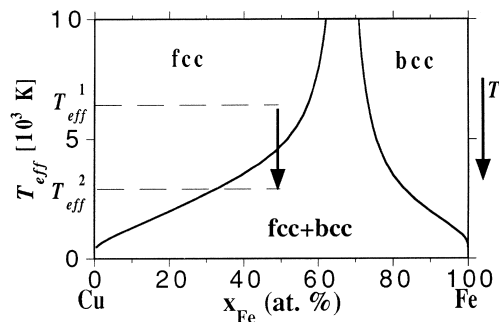


Fig. 12. Calculated dynamic Cu–Fe phase diagram in  $T_{\text{eff}}$  (see text). Arrow represents quench from  $T_{\text{eff}}^1$  to  $T_{\text{eff}}^2$ .

the possibility of large local temperature spikes counteracting the increased milling intensity, our dynamic phase diagram explains this observation. Again, because the two phases have different structure and therefore different slopes at the point of intersection, the incremental effect of increased milling intensity (and increasing effective temperature) is small at high effective temperatures. Finally, the fact that  $\Delta H(c)$  is steeper for the b.c.c. phase than for the f.c.c. phase, results in higher solubility in the latter, in qualitative agreement with previous reports [35]. It is noted that the calculated dynamic phase diagram indicates values of  $T_{\text{eff}}$  in excess of 5000 K for the solubilities observed in Cu–Fe alloys formed by high-energy ball milling.

Many attempts have been made to explain phase formation in ball-milled alloys using equilibrium thermodynamics. While some limiting cases can be rationalized using qualitative thermodynamics arguments, a complete interpretation requires consideration of the kinetic behavior. For example, a purely thermodynamic approach does not explain the two-phase region in the Cu–Fe system [7]. Although it is difficult to apply the effective-temperature theory [24] in a quantitative manner, it provides a consistent interpretation for a variety of observed transformations under ball milling. We also note that transformations from equilibrium to competing metastable phases have been suggested to occur when defect accumulation in the former raises their free energy to above that of the latter. However, consistent use of this argument would require consideration of defect accumulation in both the initial and the product phase. For example, we have observed [18] that in the Zr–Al system, the stored enthalpies in the amorphous and hexagonal phases are of similar magnitude.

The enthalpy released during DSC measurements in unstable alloys has its origins in phase decomposition, strain release and grain growth during heating of the alloys. It is difficult to separate the different contributions since they occur simultaneously. Nevertheless, it was indicated in previous studies [34, 35] that only a small amount of heat release results from grain growth and strain reduction, about 1 kJ/mol, compared with the greater heat release due to phase separation. Therefore, the stored enthalpy is a convenient measure of the degree of separation in the parent alloy [e.g. Figs 6 and 11(c)].

If one hypothetically assumes that the f.c.c. phase is chemically homogeneous during precipitation of the b.c.c. phase, the ratio of the molar fraction of the b.c.c. phase,  $\alpha$ , to that of the f.c.c. phase,  $1 - \alpha$ , can be calculated from the compositions of the phases:

$$\frac{\alpha}{1 - \alpha} = \frac{\frac{1}{2} - c_{\text{f.c.c.}}}{c_{\text{b.c.c.}} - \frac{1}{2}} \quad (3)$$

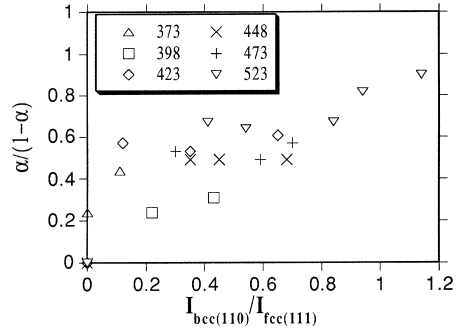


Fig. 13.  $\alpha/(1 - \alpha)$ , where  $\alpha$  is the molar fraction of the b.c.c. phase, during the initial stages of decomposition, as a function of the measured b.c.c. (110) to f.c.c. (111) peak ratio. It is calculated from the f.c.c. lattice parameter assuming a homogeneous f.c.c. phase. The temperatures are indicated in the legend.

where  $c_{\text{f.c.c.}}$  and  $c_{\text{b.c.c.}}$  are the atomic fractions of Fe in the respective phases. In Fig. 13, this ratio is plotted vs the measured b.c.c. (110) to f.c.c. (111) peak intensity ratio for the initial stages of decomposition. The composition of the f.c.c. phase has been determined from the lattice parameter using the data of Ma *et al.* [35]. Based on our observations, the Cu solubility in the b.c.c. phase is neglected. For  $T \geq 423$  K, it is obvious that compositional changes, expressed in  $\alpha/(1 - \alpha)$ , occur before a significant amount of a b.c.c. phase is present. If the assumptions used for the calculations were correct, a straight line through the origin would be expected in Fig. 13 at short times. Therefore, the observed changes in the lattice parameter are attributed to the formation of an Fe-rich f.c.c. phase, as has been observed following thermal annealing of  $\text{Cu}_{50}\text{Fe}_{50}$  [33, 36, 41–43, 52]. In addition, Mössbauer results on a parent alloy after LEBM 20 h at 448 K confirm the presence of f.c.c.-Fe. Based on magnetic measurements and TEM observations, several authors have suggested that the initial stages of decomposition of  $\text{Cu}_{50}\text{Fe}_{50}$  occur by a spinodal process in the f.c.c. phase [36, 41–44].

We note that the conclusion of the previous paragraph is possible because the lattice parameters of f.c.c.-Cu (0.3615 nm [58]) and f.c.c.-Fe (0.3588 nm [62]) are both smaller than that of  $\text{Cu}_{50}\text{Fe}_{50}$  (0.3640 nm). The lattice parameter has a maximum near the equiatomic composition, so that precipitation of either f.c.c.-Fe or b.c.c.-Fe results in a significant change in the average f.c.c. lattice parameter. Therefore, the near-absence of any Fe-rich phase in the steady state at 423 K and below, confirmed by Mössbauer spectroscopy, can also be concluded directly from the observed lattice-parameter data. The positive deviation from Vegard's law in ball-milled Cu–Fe has been attributed to elastic strain and magnetovolume effects [10] and, more recently, to bond dilation between unlike atoms [40].

It is difficult to interpret the FWHM data quantitatively since significant contributions due to chemical heterogeneity are very likely. Use of the Williamson–Hall method [63] to determine grain size and root-mean square strain has not led to consistent results. We suggest that the majority of the broadening at  $T \leq 473$  K is due to chemical heterogeneities, and further work is in progress to characterize them. At 523 K, the system is close to equilibrium, so that the amount of solute is small, as is the chemical heterogeneity. The large broadening of the b.c.c. (110) peaks for  $T \leq 423$  K is attributed to a reduction in grain size, since this phase is observed to be dissolved into the f.c.c. phase at the same time.

The comparison of precipitation kinetics with and without milling at 473 and 523 K clearly indicates the importance of milling-enhanced diffusion. Although the equilibrium phases at these temperatures are dilute terminal solutions, diffusion kinetics are sluggish and the time scale for equilibration during annealing is of the order of  $10^3$  h. While milling-induced mixing reduces the driving force for equilibration, the effect of deformation-enhanced diffusion dominates and precipitation is faster. We note that the non-monotonic behavior of the lattice parameter during annealing (Fig. 8) does not indicate reversal of precipitation, but is rather a result of the formation of f.c.c.-Fe. We arrive at this conclusion because the stored enthalpy and the b.c.c. (110) to f.c.c. (111) intensity ratio are both monotonic. Since the lattice parameters of both terminal f.c.c. solutions are significantly smaller than that of the alloy, formation of f.c.c.-Fe leads to a reduction of the average f.c.c. lattice parameter. When the f.c.c. to b.c.c. transformation occurs, the resulting increase in the average f.c.c. lattice parameter dominates over the effect of further decomposition of the f.c.c. phase, leading to a reversal in Fig. 8.

The most unexpected result is the reversal of Fe precipitation at later times, observed for milling between 373 and 473 K. At 423 K and below, the initial precipitation is reversed and the alloy is homogeneous at steady state. We now analyze the general implications of non-monotonic behavior. When a state variable  $S$  (e.g. the volume fraction of a second phase) is not a monotonic function of time, the time derivative  $dS/dt$  is double-valued for some values of  $S$  (see Fig. 14). This implies that  $dS/dt$  is not a function of  $S$  alone, but there is an *additional, time-dependent, state variable,  $u(t)$* , on which  $dS/dt$  depends. Translated to our particular example, the state of decomposition is not the only variable that determines the rate of further decomposition. This is particularly evident in the fact

that the parent alloy at  $t = 0$  is nearly identical to that milled at 423 K for longer than 150 h. Nevertheless, the former decomposes at 423 K, whereas the latter is at steady state. A time-dependent impurity concentration is a common suggestion. However, the reversibility of the steady-state, demonstrated by temperature cycling, as well as the relatively low impurity levels, make such an effect unlikely. We suggest that the additional state variable is related to the instantaneous microstructure. The grain size, alloy solubilities,<sup>†</sup> volume fractions of the different phases and the nature of the interfaces between them, all affect the mechanical properties of the powder. Since  $\mathcal{D}_{\text{Bal}}$  is a function of the mechanical properties, it is plausible that the effective temperature evolves in time and is different in nominally identical alloys. We note that while temperature and microstructure essentially do not affect  $\mathcal{D}_{\text{Bal}}$  in irradiated alloys, they do affect it significantly in ball-milled powders. We also add that we attribute the varying widths of the DSC peaks for nominally identical samples to variations in the microstructure affecting nucleation and/or growth kinetics.

Non-monotonic phase evolution during ball milling has also been observed for polymorphous crystalline–amorphous transformations [66, 67]. After mechanical alloying of Co and Ti to form an amorphous phase, the authors observed several alternating crystallization/amorphization cycles and ruled out an impurity effect as an explanation. The authors suggest that each phase is destabilized once it has accumulated milling-induced defects. We point out that in order to support this interpretation, one needs to establish that two strict requirements are satisfied: (a) the defect density in a newly formed transformation product is initially low; and (b) the transformation is abrupt, i.e. the distribution of milling times leading to destabilization is narrow compared to the cycle length. If these requirements are not satisfied, then a two-phase steady state will be reached before a cycle is completed.

It is evident in Figs 4 and 5 that the initial rate of precipitation is insensitive to the temperature for  $423 \text{ K} < T < 473 \text{ K}$ . A complete analysis of the pre-

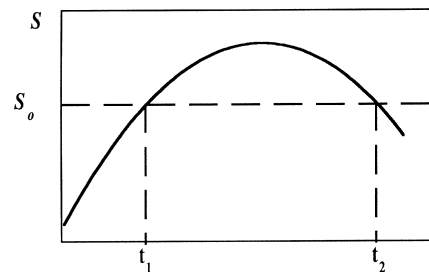


Fig. 14.  $S(t)$  is a non-monotonic function of  $t$ . At  $t_1$  and  $t_2$   $S$  has the same value, but  $dS/dt$  has different values. It follows that  $dS/dt$  is not only a function of  $S$ , but also of an additional variable.

<sup>†</sup>Depending on the phase, both solution hardening and softening have been observed in ball-milled Cu–Fe alloys. See, e.g. Refs [64, 65].

precipitation kinetics requires knowledge of both the driving force and diffusion kinetics. First consider the behavior of deformation-enhanced diffusion. Following Ref. [13], we assume a uniform vacancy generation rate,  $K_o$ , and a rate of absorption at sinks given by  $k_v^2 D_v$ , where  $D_v$  is the vacancy diffusion coefficient and  $k_v^2$ , the sink strength, which is linear in the sink density. Physically,  $K_o$  is due to nonconservative dislocation motion [26]. If the effect of vacancies is dominant, the deformation-enhanced diffusion coefficient at steady-state is given by

$$D_{\text{DED}} = D_v c_v = \frac{K_o}{k_v^2} + D_v c_v^o \quad (4)$$

where  $c_v$  and  $c_v^o$  are the vacancy concentration and its equilibrium value, respectively. At sufficiently low temperatures, when vacancies are immobile, this treatment is not valid, since it would imply an unphysically high vacancy concentration. Therefore,  $D_{\text{DED}}$  vanishes in the low-temperature limit. At intermediate temperatures, when vacancies are mobile, the second term is negligible, and the only temperature dependence of  $D_{\text{DED}}$  results from that of the deformation behavior. At higher temperatures,  $D_{\text{DED}}$  increases again due to the contribution of thermal vacancies. Assuming that the deformation behavior does not vary significantly in the range 423–473 K, this qualitative picture is consistent with the observed plateau in decomposition rate. It is difficult to compare our observations with diffusion studies in Fe because vacancy mobility is highly sensitive to the impurity content. In ultra-high-purity Fe, vacancy mobility was observed at temperatures near 200 K (e.g. Ref. [68]), whereas observed vacancy migration enthalpies in conventional-purity Fe indicate that vacancies are frozen up to significantly higher temperatures [69]. We note here that  $D_{\text{DED}}$  may behave as  $K_o$  (a function of the milling intensity) to a power less than one when equation (4) fails at high vacancy concentrations.

The variation of the driving force with temperature is more difficult to assess. As discussed earlier, the effective temperature, and with it the driving force, evolves with milling time. This evolution is obviously temperature dependent. The accuracy of the data is not sufficient to model the decomposition kinetics under a time-dependent driving force and fit such a model to the data to determine the driving force. Also, the existence of two Fe-rich phases complicates the analysis of the kinetics. Thus, the possibility remains open that the observed temperature-independent decomposition rate is due to an intricate interplay between  $D_{\text{DED}}$  and the driving force.

The lowering of the peak degree of precipitation with increasing milling intensity at 423 K suggests that the enhancement of the rate of microstructure

evolution due to increased milling intensity is greater than the enhancement in diffusivity. If both  $\tilde{\mathcal{D}}_{\text{Bal}}$  and  $\tilde{D}$  have the same dependence on the milling intensity, the effective thermodynamics are expected to be independent of the latter [equation (1)]. However, if  $\tilde{D}$  behaves as the milling intensity to a power less than one due to invalidity of equation (4) (see earlier), an increasing milling intensity will cause the effective temperature to increase, so that the driving force for segregation will decrease.

From the steady-state lattice parameters, the Fe solubility in the f.c.c. phase has been calculated as a function of temperature, assuming the phase to be homogeneous. Using equation (2),  $T_{\text{eff}}$  has been calculated, from which the ratio  $\tilde{\mathcal{D}}_{\text{Bal}}/\tilde{D}$  has been determined. An Arrhenius plot of this ratio as a function of  $1/T$  yields an apparent activation enthalpy of 0.65 eV. Since we suggest that the mechanical properties vary among samples milled at different temperatures, both  $\tilde{\mathcal{D}}_{\text{Bal}}$  and  $\tilde{D}$  are temperature dependent, and it is difficult to provide a physical interpretation of this apparent activation enthalpy.

Finally, we believe that the results of Klassen *et al.* [29] represent a particularly striking example of coupling between the phase evolution and microstructure. The authors interpret their X-ray data as indicating decomposition of a homogeneous Ag–Cu solid solution into three phases: two terminal Ag-rich and Cu-rich solid solutions, and a concentrated alloy. Alternatively, the data can be interpreted as indicating a wide distribution of compositions. We suggest the following explanation: initially, evolution toward effective equilibrium leads to precipitation of terminal solutions from the parent alloy. The ductile terminal solutions encapsulate particles of the solution-hardened parent alloy and prevents their further deformation. Consequently, deformation-enhanced diffusion in the parent alloy ceases, causing departure from effective equilibrium. We have also observed non-monotonic decomposition behavior in unstable f.c.c. Ag<sub>50</sub>Cu<sub>50</sub> [70], suggesting that the phenomenon may be common.

## 5. CONCLUSIONS

Low-energy ball milling of unstable, f.c.c. Fe<sub>50</sub>Cu<sub>50</sub> alloy powders at a temperature range of 423–523 K leads to segregation and precipitation of b.c.c.-Fe and f.c.c.-Fe. The precipitation kinetics are significantly enhanced by milling-induced deformation, despite the reduced driving force due to the homogenizing effect of the deformation. The temperature dependence of the initial decomposition rate is negligible for  $423 \text{ K} \leq T \leq 473 \text{ K}$ , but the steady-state degree of decomposition shows significant temperature dependence. A dynamic Cu–Fe phase diagram based on Martin’s effective-temperature theory provides consistent explanations of

phases observed in ball-milled Cu–Fe. In contrast to irradiated materials, the “ballistic interdiffusion coefficient” in ball-milled powder is strongly dependent on the microstructure, which results in a time-dependent effective temperature, leading to non-monotonic decomposition behavior.

*Acknowledgements*—The authors gratefully acknowledge stimulating discussions with E. Ma and K. Lian and assistance in ball milling experiments from H.-H. Tian. This work was supported by the U.S. National Science Foundation under Grant DMR-9500617. Mössbauer measurements at Washington State University were supported in part by the U.S. National Science Foundation under Grant DMR-9612306.

### REFERENCES

- Weeber, A. W. and Bakker, H., *Physica B*, 1988, **153**, 93.
- Koch, C. C., *Mater. Sci. Forum*, 1992, **88–90**, 243.
- Schultz, L. and Eckert, J., in *Glassy Metals III*, ed. H. Beck and H.-J. Güntherodt, Topics in Applied Physics, Vol. 72. Springer, Berlin, 1994, p. 69.
- Ma, E. and Atzmon, M., *Mater. Chem. Phys.*, 1995, **39**, 249.
- Bakker, H., Zhou, G. F. and Yang, H., *Prog. Mater. Sci.*, 1995, **39**, 159.
- Johnson, W. L., *Prog. Mater. Sci.*, 1986, **30**, 81.
- Eckert, J., Holzer, J. C., Krill, C. E. III and Johnson, W. L., *J. appl. Phys.*, 1993, **73**, 2794.
- Oehring, M., Yan, Z. H., Klassen, T. and Bormann, R., *Physica status solidi (a)*, 1992, **131**, 671.
- Gente, C., Oehring, M. and Bormann, R., *Phys. Rev. B*, 1993, **48**, 13244.
- Yavari, A. R., Desré, P. J. and Benameur, T., *Phys. Rev. Lett.*, 1992, **68**, 2235.
- Benjamin, J. S. and Schelleng, R. D., *Metall. Trans. A*, 1981, **12A**, 1827.
- Schwarz, R. B., Petrich, R. R. and Saw, C. K., *J. Non-Cryst. Solids*, 1985, **76**, 281.
- Sizmann, R., *J. nucl. Mater.*, 1968, **69–70**, 386.
- Baluffi, R. W. and Ruoff, A. L., *J. appl. Phys.*, 1963, **34**, 1634.
- Ruoff, A. L. and Baluffi, R. W., *J. appl. Phys.*, 1963, **34**, 1848.
- Ruoff, A. L. and Baluffi, R. W., *J. appl. Phys.*, 1963, **34**, 2862.
- Koch, C. C., Cavin, O. B., McKamey, C. G. and Scarborough, J. O., *Appl. Phys. Lett.*, 1983, **43**, 1017.
- Ma, E. and Atzmon, M., *Phys. Rev. Lett.*, 1991, **67**, 1126.
- Chen, Y., Bibole, M., Le Hazif, R. and Martin, G., *Phys. Rev. B*, 1993, **48**, 14.
- Pochet, P., Tominez, E., Chaffron, L. and Martin, G., *Phys. Rev. B*, 1995, **52**, 4006.
- Xu, J., Herr, U., Klassen, T. and Averback, R. S., *J. appl. Phys.*, 1996, **79**, 3935.
- Wei, L. C. and Averback, R. S., *J. appl. Phys.*, 1997, **81**, 613.
- Bellon, P. and Averback, R. S., *Phys. Rev. Lett.*, 1995, **74**, 1891.
- Martin, G., *Phys. Rev. B*, 1984, **30**, 1424.
- Darken, L. S., *Trans. Am. Inst. Min. Engrs*, 1948, **175**, 184.
- Arnaud, B., Le Hazif, R. and Martin, G., *Acta metall.*, 1985, **33**, 1105.
- Bocquet, J. L., Brebec, G. and Limoge, Y., in *Physical Metallurgy*, ed. R. W. Cahn and P. Haasen. North-Holland, Amsterdam, 1996, p. 634.
- Atzmon, M. and Ma, E., in *Solid–Solid Phase Transformations*, ed. W. C. Johnson, J. M. Howe, D. E. Laughlin and W. A. Soffa. TMS, Warrendale, Pennsylvania, 1994, p. 963.
- Klassen, T., Herr, U. and Averback, R. S., *Acta mater.*, 1997, **45**, 2921.
- Uenishi, K., Kobayashi, K. F., Nasu, S., Hatano, H., Ishihara, K. N. and Shingu, P. H., *Z. Metallk.*, 1992, **83**, 132.
- Gaffet, E., Harmelin, M. and Faudot, F., *J. Alloys Compounds*, 1993, **194**, 23.
- Jiang, J. Z., Gonser, U., Gente, C. and Bormann, R., *Appl. Phys. Lett.*, 1993, **63**, 1056.
- Jiang, J. Z., Gonser, U., Gente, C. and Bormann, R., *Appl. Phys. Lett.*, 1993, **63**, 2768.
- Eckert, J., Holzer, J. C. and Johnson, W. L., *J. appl. Phys.*, 1993, **73**, 131.
- Ma, E., Atzmon, M. and Pinkerton, F. E., *J. appl. Phys.*, 1993, **74**, 955.
- Drbohlav, O. and Yavari, A. R., *Acta metall. mater.*, 1995, **43**, 1799.
- Crespo, P., Hernando, A., Garcia Escorial, A., Kermner, K. M. and Harris, V. G., *J. appl. Phys.*, 1994, **76**, 6322.
- Schilling, P. J., He, J.-H., Cheng, J. and Ma, E., *Appl. Phys. Lett.*, 1996, **68**, 767.
- Ma, E., He, J.-H. and Schilling, P. J., *Phys. Rev. B*, 1997, **55**, 5542.
- Harris, V. G., Kemner, K. M., Das, B. N., Koon, N. C., Ehrlich, A. E., Kirkland, J. P., Woicik, J. C., Crespo, P., Hernando, A. and Garcia Escorial, A., *Phys. Rev. B*, 1996, **54**, 6929.
- Crespo, P., Hernando, A. and Garcia Escorial, A., *Phys. Rev. B*, 1994, **49**, 13227.
- Crespo, P., Hernando, A., Yavari, R., Drbohlav, O. and Garcia Escorial, A., *Phys. Rev. B*, 1993, **48**, 7134.
- Hernando, A., Crespo, P., Garcia Escorial, A., Barandilaran, J. M., Urchulutegui, M. and Vittori Antisari, M., *Europhys. Lett.*, 1995, **32**, 585.
- Mazzone, G. and Vittori Antisari, M., *Phys. Rev. B*, 1996, **54**, 441.
- Macri, P. P., Rose, P., Frattini, R., Enzo, S., Principi, G., Hu, W. X. and Cowlam, N., *J. appl. Phys.*, 1994, **76**, 4061.
- Macri, P. P., Enzo, S., Cowlam, N., Frattini, R., Principi, G. and Hu, W. X., *Phil. Mag. B*, 1995, **71**, 249.
- Huang, J. Y., He, A. Q. and Wu, Y. K., *Nanostruct. Mater.*, 1994, **4**, 1.
- Huang, J. Y., He, A. Q., Wu, Y. K., Ye, H. Q. and Li, D. X., *J. Mater. Sci.*, 1996, **31**, 4165.
- Huang, J. Y., Yu, Y. D., Wu, Y. K., Li, D. X. and Ye, H. Q., *Acta mater.*, 1997, **45**, 113.
- Fultz, B., Ahn, C. C., Spooner, S., Hong, L. B., Eckert, J. and Johnson, W. L., *Metall. Mater. Trans. A*, 1996, **27A**, 2934.
- Hong, L. B. and Fultz, B., *Acta mater.*, 1998, **46**, 2937.
- Huang, J. Y., Yu, Y. D., Wu, Y. K., Ye, H. Q. and Dong, Z. F., *J. Mater. Res.*, 1996, **11**, 2717.
- Schwarz, R. B. and Koch, C. C., *Appl. Phys. Lett.*, 1986, **49**, 146.
- Davis, R. M., McDermott, B. and Koch, C. C., *Metall. Trans. A*, 1988, **19A**, 2867.
- Chen, Y., Le Hazif, R. and Martin, G., *Diffusion Defect Data—Solid State Data, Part B*, 1992, **23**, 271.
- Klug, H. P. and Alexander, L., in *X-ray Diffraction Procedures for Polycrystalline and Amorphous Materials*, 2nd edn. Wiley, New York, 1974, p. 661.
- Greenwood, N. N. and Gibb, T. C., *Mossbauer Spectroscopy*. Chapman & Hall, London, 1971.

58. *CRC Handbook of Chemistry and Physics*, 65th edn. CRC Press, Boca Raton, 1984, p. B-203.
59. Warren, B. E., *X-ray Diffraction*. Dover, New York, 1990, p. 253.
60. Michaelsen, C., *Phil. Mag. A*, 1985, **72**, 813.
61. Sumiyama, K. *et al.*, *Acta metall.*, 1985, **33**, 1785.
62. Newkirk, J. B., *Trans. Am. Inst. Min. Engrs*, 1957, **209**, 1214.
63. Williamson, G. K. and Hall, W. H., *Acta metall.*, 1953, **1**, 22.
64. Shen, T. D. and Koch, C. C., *Acta mater.*, 1996, **44**, 753.
65. Zhu, M. and Fecht, H.-J., *Nanostruct. Mater.*, 1995, **6**, 921.
66. El Eskandarany, M. S., Aoki, K., Sumiyama, K. and Suzuki, K., *Appl. Phys. Lett.*, 1997, **70**, 1679.
67. El Eskandarany, M. S., Aoki, K., Sumiyama, K. and Suzuki, K., *Scripta mater.*, 1997, **36**, 1001.
68. Takaki, S., Fuss, J., Kugler, H., Dedek, U. and Schultz, H., *Rad. Eff.*, 1982, **79**, 78.
69. Ehrhart, P., in *Atomic Defects in Metals*, Landolt-Boernstein, New Series, Group 3, Vol. 25. Springer, Berlin, 1991.
70. Tian, H. H. and Atzmon, M., 1999, **47**, 1255.